

Angular and energy dependence of (e, e') cross sections for orbital 1^+ excitations

R. Nojarov*, Amand Faessler[†] and M. Dingfelder[‡]

Institut für Theoretische Physik, Universität Tübingen,
Auf der Morgenstelle 14, D-72076 Tübingen, Germany

August 11, 2018

Abstract

The main features of the (e, e') cross sections of low-lying orbital excitations with $K^\pi = 1^+$ in heavy deformed nuclei are studied in RPA on the example of ^{156}Gd . The dependence of the DWBA E2 and M1 cross sections on the scattering angle $0^\circ < \theta < 180^\circ$ and incident electron energy $E_i < 210$ MeV is analyzed in PWBA. The cross section is larger for M1 than for E2 transitions at any angle if $E_i < 30$ MeV. The longitudinal (Coulomb) C2 excitation dominates the E2 response for $5^\circ < \theta < 170^\circ$. Only transverse M1 and E2 excitations compete for $\theta > 175^\circ$ and the former one is dominant for $q < 1.2 \text{ fm}^{-1}$. The M1 response is almost purely orbital up to $q = 1.4 \text{ fm}^{-1}$ even in backward scattering. Qualitative PWBA estimates based on the q -dependence of the form factors alone are not able to predict some important features of the (e, e') cross sections stemming from the strong magnetic and orbital character of the studied 1^+ excitations. The expectation for M1 over E2 dominance in backward scattering should not be extended to higher momentum transfers and incident energies.

*Permanent address: Institute for Nuclear Research and Nuclear Energy, Bulgarian Academy of Sciences, BG-1784, Sofia, Bulgaria. E-mail: roland.nojarov@uni-tuebingen.de

[†]E-mail: amand.faessler@uni-tuebingen.de

[‡]E-mail: michael.dingfelder@uni-tuebingen.de

1 Introduction

The backward inelastic electron scattering has established itself in the last 30 years as one of the main tools for the experimental study of nuclear magnetic excitations. The attention was focused in the past mainly on spherical nuclei, as it can be seen, e.g., from the review articles [1, 2]. The detailed study of low-lying magnetic dipole (M1) excitations in heavy deformed nuclei started with (e, e') experiments at the linear accelerator in Darmstadt [3], reviewed recently in [4]. Most of the data were collected at a backward scattering angle $\theta = 165^\circ$, where one expects a strong damping of electric excitations.

This can be understood from qualitative considerations [5, 6] in the plane wave Born approximation (PWBA). The (e, e') cross section can be decomposed in this case into longitudinal (Coulomb) and transverse (electric and magnetic) terms, multiplied by corresponding kinematic factors. The longitudinal kinematic factor $V_\ell(\theta)$ vanishes for $\theta = 180^\circ$ and only transverse multipoles are excited in backward scattering [5]. Among those with the same multipolarity, the magnetic excitation is dominant over the electric transverse one [6]. This qualitative estimate is obtained in the long-wave limit $qR \ll 1$, or small momentum transfer q in comparison with the radius R of the target nucleus. Magnetic dominance was found at backward angle also in [1] by assuming a purely spin-flip transition.

The more realistic distorted wave Born approximation (DWBA) [7] leads to important corrections especially in heavy nuclei with a strong Coulomb field (a large charge number Z). But this approach is not suitable for simple qualitative predictions, since the longitudinal and transverse electric contributions to the (e, e') cross section interfere with each other in DWBA. Moreover, their separation would be meaningless when the longitudinal and transverse electric contributions are related in the DWBA formalism [8, 9] through the continuity equation.

In contrast to the above discussed common expectations based on the PWBA, we have found recently [10, 11] E2 contributions to the cross sections of low-lying orbital M1 excitations measured at $\theta = 165^\circ$. Such admixtures take place in heavy deformed nuclei where the M1 transition with $I^\pi K = 1^+1$ is accompanied by a closely lying E2 transition with $I^\pi K = 2^+1$ to the first member of the rotational band built on the intrinsic $K^\pi = 1^+$ excitation. The large moment of inertia of these nuclei leads to a small separation

between the two excitation energies, comparable with the energy resolution of the (e, e') experiments. The accompanying E2 transition provides an important contribution to the measured cross sections ($\theta = 165^\circ$) for an effective momentum transfer $0.6 < q_{\text{eff}} < 0.9 \text{ fm}^{-1}$ corresponding to incident electron energies in the range $40 < E_i < 70 \text{ MeV}$ [10, 11].

The M1 excitations in spherical nuclei are mainly of spin-flip type, which is expected to be favoured in backward electron scattering [2]. In contrast, we are considering here a qualitatively different type of predominantly orbital M1 excitations. They appear only in deformed nuclei [12] and their experimental study through backward (e, e') scattering started much later [3, 4].

We are going to examine here in more detail some of the well-known qualitative PWBA predictions for the interplay of magnetic and electric excitations, paying attention also to the approximations involved. These predictions ignore the nuclear dynamics because they are made for the general case of unknown transition densities. The latter could exhibit however some important peculiarities, typical for the considered nuclear excitations. The qualitative PWBA estimates will be compared here to DWBA and PWBA cross sections obtained from realistic RPA transition densities in order to understand to what extent one could use the general PWBA predictions for qualitative interpretation of realistic microscopic results.

We shall study to this purpose the dependence of our theoretical DWBA (e, e') cross sections on the electron incident energy and momentum transfer in the whole possible range of scattering angles $0^\circ < \theta < 180^\circ$. Cross sections of 1^+ excitations in deformed nuclei have been presented and discussed until now almost exclusively for $\theta = 165^\circ$ in order to compare them with the corresponding experimental data measured at this angle. Only the cross section of the strongest (low-lying orbital) M1 excitation is known experimentally in each one of the several heavy deformed nuclei studied until now. We choose here ^{156}Gd as an example, because this is the only nucleus, where the accompanying E2 transition was identified experimentally [13].

We shall present and discuss in the next section the dependence of E2 and M1 cross sections of this typical 1^+ excitation on the incident electron energy and momentum transfer in the whole range of scattering angles. The results are analyzed qualitatively in PWBA for small and large momentum transfer in sections 3 and 4, respectively. The

conclusions are summarized in sect. 5 and expressions for E2 transition densities are given in the Appendix.

2 Angular and energy dependence of E2 and M1 (e, e') cross sections

We describe intrinsic excitations with $K^\pi = 1^+$ in deformed nuclei within the quasiparticle random phase approximation (QRPA, or shorter RPA) using a model hamiltonian specified in [14]. It contains a quasiparticle (q.p.) mean field, given by a deformed Woods-Saxon potential plus pairing. The separable residual interaction consists of a spin-spin force and a quadrupole-type interaction, derived self-consistently from the deformation of the mean field. The isoscalar coupling constant of the latter interaction, determined microscopically, ensures the rotational invariance of the model hamiltonian, which is violated by the mean field alone.

The choice of the parameters of the model hamiltonian is explained in more detail elsewhere [14]. In contrast to many other microscopic calculations, energies of single-particle levels are not shifted but taken exactly as provided by the deformed Woods-Saxon potential. Expressions for M1 and E2 transition probabilities in terms of the RPA amplitudes are given in [15]. The large single-particle basis allows us to work without effective charges ε_{eff} when calculating $B(E2; 0^+0 \rightarrow 2^+1)$ values and E2 transition densities. The $B(M1; 0^+0 \rightarrow 1^+1)$ values and M1 transition densities are obtained with bare orbital and effective spin gyromagnetic factors. The latter account for the renormalization of the spin operator by a factor of 0.7, i.e.,

$$\varepsilon^n = 0, \quad \varepsilon^p = 1, \quad g_j^s = 0.7g_j^s(\text{free}), \quad g_n^s(\text{free}) = -3.8263, \quad g_p^s(\text{free}) = 5.5858. \quad (1)$$

The strongest M1 transition found experimentally in ^{156}Gd has an excitation energy $E_x = 3.07$ MeV and a reduced magnetic transition probability $B(M1) = 1.30 \pm 0.20 \mu_N^2$ [16]. It is easily identified with the strongest theoretical M1 transition at 2.90 MeV with $B(M1) = 1.24 \mu_N^2$. Our theoretical reduced probability for the accompanying E2 transition, $B(E2) = 42 \text{ e}^2\text{fm}^4$, agrees also well with the corresponding experimental value $40 \pm 6 \text{ e}^2\text{fm}^4$ [13]. The $B(E2)$ values of $K^\pi = 1^+$ excitations are small because the main

collectivity of the E2 strength of this mode is concentrated in the spurious rotational state, i.e. in the lowest E2 transition of the ground state rotational band.

The (e, e') cross sections are, however, much more sensitive to the details of the RPA wave functions than transition probabilities or excitation energies. We obtain the transition densities, necessary for the calculation of DWBA cross sections, as reduced matrix elements of the corresponding multipole density operators between the nuclear ground state and the ν -th RPA excitation with $I^\pi K = L^+1$ ($L = 1, 2$):

$$\rho_2^\nu(r) = \langle 2^+1, \nu \parallel \hat{\rho}_2^\dagger(r) \parallel 0 \rangle, \quad (2)$$

$$\mathcal{J}_{LL'}^\nu(r) = i\langle L^+1, \nu \parallel \hat{\mathcal{J}}_{LL'}^\dagger(r) \parallel 0 \rangle, \quad \mathcal{J}_{LL'}^\nu(r) = \mathcal{J}_{LL'}^{\nu,C}(r) + \mathcal{J}_{LL'}^{\nu,S}(r), \quad (3)$$

where $\hat{\rho}_2(r)$ and $\hat{\mathcal{J}}_{LL'}(r)$ are longitudinal charge (C2) and transverse current (TL) density operators, respectively. The latter reduce to $\hat{\mathcal{J}}_{11}(r)$ for M1 excitations ($L = L' = 1$) and $\hat{\mathcal{J}}_{2L'}(r)$ for E2 excitations ($L = 2, L' = 1, 3$). The transverse (current) transition densities $\mathcal{J}_{LL'}^\nu(r)$ are written in (3) as a sum of two terms originating from the proton convection current density $\hat{\mathbf{j}}^C(\mathbf{r})$ and the magnetization (or spin) current density $\hat{\mathbf{j}}^S(\mathbf{r})$ of protons and neutrons.

The current density operators and expressions for the M1 transition densities in RPA can be found in [17]. Expressions for the E2 transition densities are given in the Appendix. The (e, e') cross sections are calculated numerically from the transition densities (2), (3), using the DWBA formalism described in [8, 9].

The theoretical DWBA cross sections of the above described low-lying orbital 1^+ excitation in ^{156}Gd are displayed in Figs. 1 and 2. The M1 and E2 (e, e') cross sections are plotted in Fig. 1 versus the incident electron energy in the range $10 \leq E_i \leq 210$ MeV and scattering angles $5^\circ \leq \theta \leq 175^\circ$.

Since we are interested here mainly in qualitative conclusions, the agreement with experiment is relevant to the extent it could promote the confidence in the theoretical cross sections beyond the experimentally studied scattering angle of 165° . Two-dimensional sections of the three-dimensional plots in Fig. 1, corresponding to a fixed angle $\theta = 165^\circ$ and $E_i < 100$ MeV, were plotted together in [11] and compared with experimental data [3], taken at this angle. The E2 excitation provides important contributions to the measured M1 cross section in the region $40 < E_i < 70$ MeV and leads to a very good agreement with experiment after being taken into account.

These features can be seen also by comparing the shaded areas ($\theta = 175^\circ$) of the M1 and E2 cross sections in Fig. 1. For small incident energies E_i the E2 cross section is two orders of magnitude smaller than the M1 cross section but both are comparable at higher E_i . At 175° the two cross sections are comparable for $120 < E_i < 200$ MeV and the E2 response is dominant for $E_i > 200$ MeV.

We are going to analyze qualitatively our microscopic DWBA cross sections using PWBA, where the cross section can be decomposed into a sum of longitudinal and transverse terms [7, 8]:

$$\left(\frac{d\sigma}{d\Omega}\right)_{\text{PWBA}} = \left(\frac{Ze^2}{E_i}\right)^2 \{V_\ell |F_L^C(q)|^2 + V_t [|F_L^E(q)|^2 + |F_L^M(q)|^2]\}, \quad (4)$$

$$V_\ell = \frac{\cos^2(\theta/2)}{4\sin^4(\theta/2)}, \quad V_t = \frac{1 + \sin^2(\theta/2)}{8\sin^4(\theta/2)}, \quad V_T = V_t/V_\ell = \frac{1}{2} + \tan^2(\theta/2). \quad (5)$$

Z and $e = \sqrt{\alpha\hbar c}$ are the nuclear proton number and the unit charge, respectively. The factor $4\pi/Z^2$ from [7, 8] is incorporated in our definitions [17] of the form factors $|F_L(q)|^2$ (4), coinciding with those of [6]. Only the term $F_1^M(q)$ survives in (4) in the case of $M1$ transitions, while the $E2$ excitations are specified by longitudinal (Coulomb) $F_2^C(q)$ and transverse electric $F_2^E(q)$ contributions. The transferred momentum has in our notations the inverse dimension of length, q (fm^{-1}).

The PWBA formalism is used in this paper for two different purposes. First, in addition to the DWBA results, cross sections are calculated in some cases also in PWBA with the same RPA transition densities in order to separate the longitudinal C2 from the transverse E2 response and compare them with the transverse M1 cross sections. This separation is not possible in DWBA. Hence, the theoretical PWBA cross sections are used only as a tool for studying different constituents of the cross sections and their origin. Secondly, DWBA and PWBA cross sections, both obtained from realistic RPA transition densities, are compared to qualitative PWBA predictions which ignore completely the nuclear dynamics. These estimates are based on general considerations of the scattering kinematics and the momentum dependence of the unknown form factors. On the other hand, the latter are fully specified in our formalism by the microscopic transition densities (2), (3).

It is seen from Fig. 1 that for small incident energies the $M1$ cross section remains almost constant when going from backward to forward angles. It starts to increase for

$\theta < 90^\circ$ but, contrary to what should be expected from the diverging transverse kinematic factor V_t (5), the $M1$ cross section does not diverge in the limit $\theta \rightarrow 0^\circ$. The expressions (5), derived in the relativistic limit (neglected electron rest mass), must be corrected for extreme forward or backward angles and acquire finite values, as we shall see in the next section. The DWBA cross section of the accompanying $E2$ transition, displayed in Fig. 1, decreases substantially in the backward direction (large θ) for small incident energies. This is an indication for a dominant Coulomb response which is damped by the longitudinal factor V_ℓ at backward angles.

DWBA cross sections are plotted usually [7, 9] versus the effective momentum transfer q_{eff} ,

$$q_{\text{eff}} = q \left[1 + \frac{3}{2} \frac{Z\alpha\hbar c}{E_i R_{\text{eq}}} \right], \quad q = \frac{2}{\hbar c} \sqrt{E_i E_f} \sin(\theta/2) = \frac{2E_i}{\hbar c} \sin(\theta/2) \sqrt{1 - (E_x/E_i)}, \quad (6)$$

in order to be compared with PWBA cross sections plotted versus q . In the above expression $E_f = E_i - E_x$ is the energy of the outgoing electron. The definition (6) coincides with the formula for q_{eff} in [17] used to plot the experimental cross sections when a radius constant $r_{\text{eq}} = 1.12 \text{ fm}$ [8] is assumed in (6) for the equivalent nuclear radius $R_{\text{eq}} = r_{\text{eq}} A^{1/3}$.

The form factors $|F_L(q)|^2$ (4) are Fourier transforms of the transition densities (2), (3) with Bessel functions $j_L(qr)$ [7, 9]. Therefore, the explicit dependence of the theoretical $M1$ and $E2$ cross sections on the momentum transfer is also of prime interest. It is plotted in Fig. 2 versus q_{eff} (6) and the scattering angle θ . The indented edges in Fig. 2 result simply from the adopted finite grid of mesh points. The graph cut-off at the edge corresponds to the maximal incident energy $E_i = 200 \text{ MeV}$ included in calculations.

Let us rewrite the kinematic factors in a form that is more appropriate for a constant q . We neglect the small term E_x/E_i in (6) and express E_i^{-2} in (4) through q :

$$q = \frac{2E_i}{\hbar c} \sin(\theta/2), \quad (7)$$

$$\begin{aligned} \frac{V_\ell}{E_i^2} &= \frac{1}{q^2} [\sin^{-2}(\theta/2) - 1], & \frac{V_t}{E_i^2} &= \frac{1}{2q^2} [\sin^{-2}(\theta/2) + 1], \\ d\sigma_\ell(\theta) &= d\sigma_\ell(90^\circ) \cot^2(\theta/2), & d\sigma_t(\theta) &= d\sigma_t(90^\circ) \frac{1}{3} \left[\frac{1}{\sin^2(\theta/2)} + 1 \right]. \end{aligned} \quad (8)$$

These expressions give the angular dependence of longitudinal and transverse cross sections for a fixed momentum transfer q . It is seen from (8) that for a given q the transverse cross section decreases only 33% between 90° and 180° . In contrast, the longitudinal

cross section decreases in comparison with its value at 90° : 58 times at 165° , where most experiments were done, and 5835 times at the largest accessible backward angle of 178.5° [18].

Thus, the almost constant M1 cross section in Fig. 2 for a given momentum transfer is a typical behaviour of transverse excitations, while the steep decrease of the E2 cross section towards backward angles is an indication for a predominant longitudinal (Coulomb) component.

3 PWBA analysis for small momentum transfer

The low- q limit $qR < 1$ is reached in the considered heavy nuclei with $R \approx 6.5$ fm for very small momentum transfer $q < 0.15$ fm $^{-1}$. The PWBA cross section (4) is obtained in the relativistic limit, i.e. the electron rest mass $m_e c^2 = 0.511$ MeV is neglected in comparison with the incident electron energy E_i and a small excitation energy $E_x \ll q\hbar c$ is assumed in comparison with the momentum transfer. The former condition is always satisfied in our calculations because $E_i > 10$ MeV. The latter condition is violated at small angles, where one has to use the more accurate expressions provided by Eqs. (4-16c) and (6-38) of ref. [7]:

$$V_T = \frac{q^2}{\Delta^2} \left[\frac{1}{2} + \frac{q^2}{\Delta^2} \tan^2(\theta/2) \right], \quad \Delta^2 = q^2 - (E_x/\hbar c)^2, \quad (9)$$

$$\text{for } \theta = 0^\circ : \quad V_\ell = 4 \left(\frac{E_i}{E_x} \right)^4, \quad V_t = \frac{2E_i^6}{E_x^4(m_e c^2)^2}, \quad V_T = \frac{1}{2} \left(\frac{E_i}{m_e c^2} \right)^2. \quad (10)$$

The electron rest mass is still neglected in (9), which can not be used for $\theta = 0$ since the four-momentum is $\Delta = 0$ and the transverse factor diverges. After taking the electron mass into account, one obtains $\Delta^2(\theta = 0) = (m_e c^2 E_x / E_i)^2$ and the finite values (10) in the forward direction. The transverse cross section is strongly dominant for any realistic incident energy $E_i \gg E_x > m_e c^2$, as seen from (10). The limit (10) is however not necessary even for a very small but different from zero angle (a fraction of the degree) because the expression (9) provides already a very good numerical accuracy [19, 7]. The smallest angle displayed in the three-dimensional graphs is $\theta = 5^\circ$.

It is seen from (9) that V_T is a very large number for small angles where q is close to the photon point $E_x/\hbar c$ and Δ is small. One can understand in this way the behaviour of

the M1 and E2 cross sections at small scattering angles, exhibited in Fig. 1. The M1 cross section is dominant in the forward direction, in line with the general expectations [20, 7] for suppression of the longitudinal response through its small kinematic factor at small angles. But this is no more true for higher momentum transfer. The factor V_T (9) that damps the longitudinal (Coulomb) excitation is large at $\theta = 5^\circ$ only for small momentum transfer. However, Eq. (9) reduces already to the simpler estimate (5) $V_T \approx 0.5$ for $E_i = 200$ MeV. The Coulomb response is favoured in this case and the E2 cross section is comparable in magnitude with the M1 cross section.

The interplay between longitudinal and transverse E2 components in the forward direction can be seen in more details in Fig. 3, where the PWBA E2 cross sections are plotted versus the incident electron energy for different small scattering angles. The PWBA cross sections are obtained from the same realistic RPA transition densities of the considered 1^+ excitation in ^{156}Gd , which were used to obtain the DWBA results presented in Figs. 1 and 2. It is seen from Fig. 3 that the transverse E2 cross section (dotted lines) is almost constant and independent of the incident energy E_i , while the Coulomb cross section (dashed curves) is increasing quadratically with E_i .

The E2 cross section is purely transverse for $\theta = 0.1^\circ$ and 0.5° in the whole range ($10 < E_i < 210$ MeV) of incident energies studied. In contrast, the Coulomb term dominates for $E_i > 150$ MeV at $\theta = 1^\circ$ and for $E_i > 30$ MeV at $\theta = 5^\circ$. Its strong increase with E_i in the latter case is seen also in the DWBA E2 cross section plotted in Fig. 1. This behaviour can be understood by rewriting the PWBA cross section (4) with the help of (7) and (8):

$$\left(\frac{d\sigma}{d\Omega}\right)_{\text{PWBA}} = \left(\frac{\alpha Z}{q}\right)^2 \left\{ W_\ell |F_L^C(q)|^2 + W_t \left[|F_L^E(q)|^2 + |F_L^M(q)|^2 \right] \right\},$$

$$W_\ell = \cot^2(\theta/2), \quad W_t = \frac{1 + \sin^2(\theta/2)}{2 \sin^2(\theta/2)}, \quad W_t/W_\ell = V_T. \quad (11)$$

The q -dependence of the form factors $|F_L(q)|^2$ (11) is estimated in PWBA by taking the leading terms (lowest L) of the corresponding multipole operators into account [19]. The Bessel functions are approximated afterwards in the long-wave limit (small q) as $j_L(qr) \sim (qr)^L$, so that their contribution to the form factors is $\sim (qR)^L$ [6, 19, 7], where R is the nuclear radius. The transverse operators have convection and spin parts (3). It turns out that both parts exhibit the same leading q -dependence for magnetic, but not

for electric operators [7].

The choice of Willey [19] for the leading electric term is objected by Überall [7] who notes that only the spin term was considered in [19]. Willey has, however, both terms in view when deciding to neglect $E_x/q\hbar c$ in favour of $q\hbar c/Mc^2$, where M is the nucleon mass. Thus, the choice of Willey will be correct for $q \gg q_0$, where

$$q_0^2 = E_x Mc^2 / (\hbar c)^2 = 0.024 E_x \text{ fm}^{-2} \quad (12)$$

and the excitation energy E_x must be supplied in MeV. We obtain $q_0 = 0.27 \text{ fm}^{-1}$ for the low-energy orbital M1 excitations with $E_x \approx 3 \text{ MeV}$, studied here. Therefore, in our case we agree with the choice of Überall for the leading convection electric term in the low- q limit, while the choice of Willey remains valid for the spin current where the problem of two competing leading terms does not arise.

After introducing the above discussed correction, we obtain in the low- q limit from the expressions (2.64) for multipole operators in Ref. [19] the following estimates for the q -dependence of the PWBA form factors (11):

$$\begin{aligned} |F_L^C(q)|^2 &\sim (qR)^{2L}, & |F_L^E(q)|_{\text{conv}}^2 &\sim \left(\frac{E_x}{q\hbar c}\right)^2 (qR)^{2L}, \\ |F_L^E(q)|_{\text{spin}}^2 &\sim \left(\frac{q\hbar c}{Mc^2}\right)^2 (qR)^{2L}, & |F_{L-1}^M(q)|^2 &\sim \left(\frac{q\hbar c}{Mc^2}\right)^2 (qR)^{2L-4}. \end{aligned} \quad (13)$$

Upon insertion of (13) into (11), we get the following estimates for the PWBA cross sections in the low- q limit:

$$\begin{aligned} d\sigma(CL) &\sim (qR)^{2L-2} R^2 W_\ell, \\ d\sigma(EL, \text{conv}) &\sim \left(\frac{E_x}{\hbar c}\right)^2 (qR)^{2L-4} R^4 W_t, & \text{for } q < q_0, \\ &\sim d\sigma(EL, \text{spin}), & \text{for } q > q_0, \\ d\sigma(EL, \text{spin}) &\sim \left(\frac{\hbar c}{Mc^2}\right)^2 (qR)^{2L} W_t, \\ d\sigma(ML) &\sim \left(\frac{\hbar c}{Mc^2}\right)^2 (qR)^{2L-2} W_t, \end{aligned} \quad (14)$$

where q_0 is defined in (12). The expression for the magnetic cross section applies to both convection and spin current contributions. Although the above estimates (14) are in agreement with previous results [19, 7], the q -dependence in (14) is qualitatively different. This can be seen by comparison, e.g. with Table XXIV of [7]. The difference arises from the q -dependence of E_i^{-2} (4), expressed explicitly in (11) through (7). The previous

PWBA estimates for the q -dependence of the cross sections are valid only for a fixed incident energy, i.e. they are meaningful when the angular dependence of the form factor is studied for a constant incident energy. The scattering angle is however fixed in modern experiments [4, 2] and the form factor is studied by measurements for different incident energies. One has to apply in this case the estimates (14). They are more general since they are valid also for a fixed incident energy. The angular dependence is given in this case by the kinematic factors W (11).

We obtain from (14) the following estimates for the considered M1 and E2 PWBA cross sections by choosing the low- q limit of the convection E2 excitation:

$$\begin{aligned} d\sigma(C2) &\sim q^2 R^4 W_\ell, & d\sigma(E2, \text{conv}) &\sim \left(\frac{E_x}{\hbar c}\right)^2 R^4 W_t, \\ d\sigma(E2, \text{spin}) &\sim \left(\frac{\hbar c}{Mc^2}\right)^2 (qR)^4 W_t, & d\sigma(M1) &\sim \left(\frac{\hbar c}{Mc^2}\right)^2 W_t. \end{aligned} \quad (15)$$

Turning back to the inspection of Fig. 3, we see from (15) that the quadratic q -dependence of the Coulomb E2 excitation (dashed curves) agrees with the PWBA prediction (15). Moreover, it becomes clear that the constant transverse E2 cross section (dotted lines) must originate from a dominant convection current, because the transverse spin current would exhibit a strong q^4 -dependence. Let us note that the previous estimates [19, 7] would not be able to explain the constant transverse cross section of Fig. 3, because they predict q^2 and q^6 dependencies for the convection and spin E2 cross sections, respectively.

The following qualitative estimates for the relative transverse contributions are obtained directly from (14):

$$\frac{d\sigma(EL, \text{conv})}{d\sigma(EL, \text{spin})} \approx \left(\frac{E_x Mc^2}{(q\hbar c)^2}\right)^2 > 1, \quad \text{for } q < q_0, \quad (16)$$

$$\frac{d\sigma(M, L-1)}{d\sigma(EL, \text{spin})} \approx (qR)^{-4}, \quad (17)$$

$$\frac{d\sigma(M, L-1)}{d\sigma(EL, \text{conv})} \approx \left(\frac{(\hbar c)^2}{E_x R^2 Mc^2}\right)^2 \approx E_x^{-2}, \quad (18)$$

where q_0 is defined in (12) and a nuclear radius $R = 6.5$ fm was assumed for the rare-earth region to evaluate numerically the latter relationship in (18), valid when the excitation energy E_x is given in MeV. The ratios (16)-(18) should hold for any scattering angle. They apply to both the convection and spin parts of the magnetic excitation $(M, L-1)$. It is seen from (16) that the convection electric cross section dominates over the spin

electric one since it is taken from (14) just in the low- q limit $q < q_0$, necessary to ensure its dominance. Hence, the longitudinal cross section has to be compared only with the transverse magnetic and convection electric ones:

$$\frac{d\sigma(CL)}{d\sigma(EL, \text{conv})} \approx \left(\frac{q\hbar c}{E_x}\right)^2 \frac{1}{V_T}, \quad (19)$$

$$\frac{d\sigma(CL)}{d\sigma(M, L-1)} \approx \left(\frac{RMc^2}{\hbar c}\right)^2 \frac{(qR)^2}{V_T}. \quad (20)$$

After inserting $V_T(0^\circ)$ from (10) in the above relationships and taking into account that $q\hbar c = E_x$ at the photon point, one can easily verify that the cross section is dominated by transverse excitations at $\theta = 0^\circ$ and the longitudinal contribution is negligible:

$$\begin{aligned} \frac{d\sigma(CL)}{d\sigma(EL, \text{conv})}(0^\circ) &\approx 2\left(\frac{m_e c^2}{E_i}\right)^2 \ll 1, \\ \frac{d\sigma(CL)}{d\sigma(M, L-1)}(0^\circ) &\approx 2\left(\frac{Mm_e c^4 R^2 E_x}{(\hbar c)^2 E_i}\right)^2 \approx 2\left(\frac{m_e c^2 E_x}{E_i}\right)^2 \ll 1, \end{aligned} \quad (21)$$

where the same numerical estimate was used in the last relationship as in (18). This particular case of extreme forward scattering was discussed already above. Let us check now the predictions (17)-(20) by comparison with realistic results.

The PWBA cross sections displayed in Fig. 4 are plotted versus the transferred momentum q for $\theta = 70.53^\circ$. This angle ensures $V_T = 1$, as seen from Eq. (5), i.e. a kinematic condition which is equally favourable for both longitudinal and transverse excitations. The PWBA plots represent therefore the form factors $|F_L(q)|^2$ (4), (11) up to a coefficient common for all of them. The cross sections are calculated with our microscopic RPA transition densities for the strongest low-lying orbital 1^+ excitation in ^{156}Gd . The ratio between the orbital and spin transition matrix elements of the M1 operator [15] is $R_{o.s.} = 7.8$ for this excitation, i.e. it has a predominant orbital nature.

The PWBA M1 cross section is displayed as a continuous curve in the top plot of Fig. 4, together with the orbital contribution alone (dashed curve). This corresponds to the decomposition of the current transition density $\mathcal{J}_{11}^\nu(r)$ (3) into convection (orbital) and magnetization (spin) parts. It is seen that the M1 cross section is almost purely orbital in the considered q -range with negligible spin contributions. This is a typical property of the studied orbital 1^+ excitations in heavy deformed nuclei [12]. The predominant orbital nature at the photon point (see $R_{o.s.}$ above) is preserved up to $q = 1.4 \text{ fm}^{-1}$, as seen from Fig. 4.

This typical feature, determined by the nuclear dynamics, is not present in the qualitative PWBA estimates (13), (14), where the nuclear orbital, spin, and charge transition matrix elements are assumed to be all of comparable magnitude. The transverse E2 cross section should be one order of magnitude larger than the M1 cross section, as predicted by (18) for the considered 1^+ excitations with $E_x \approx 3$ MeV. Comparison of the upper two plots in Fig. 4 invalidates this PWBA prediction because the M1 cross section is two orders of magnitude larger than the transverse E2 contribution. This is observed also in the plots of Fig. 5, where the M1 cross section is larger than the E2 contribution for small scattering angles. The E2 cross section arises in this case mainly from the transverse E2 excitation, as one can check from Fig. 3 for small angles and small incident energies.

Let us verify now the predictions (19), (20). It is seen from the middle plot of Fig. 4 that for small q the PWBA Coulomb (C2) cross section (continuous curve) is more than one order of magnitude larger than the transverse E2 cross section (dashed curve), as it should be expected from (19) for $E_x \approx 3$ MeV.

Comparison of the upper two plots in Fig. 4 shows that the M1 response dominates over the C2 cross section only for small momentum transfer $q < 0.17 \text{ fm}^{-1}$ ($E_i < 30$ MeV). This crossing point, where the M1 and C2 cross sections are equal, is confirmed also by more realistic DWBA results, displayed in the bottom plot of Fig. 4 (note that they are plotted versus q_{eff}). On the other hand, Eq. (20) predicts that the crossing should take place for $q = 0.005 \text{ fm}^{-1}$ or $E_i = 0.85$ MeV, which is impossible since the incident energy must be larger than the excitation energy $E_x \approx 3$ MeV. Therefore, the PWBA prediction (20) overestimates the C2 with respect to the M1 cross section by three orders of magnitude.

In order to study this problem in more detail, we compare in Fig. 5 M1 and E2 DWBA cross sections plotted versus the scattering angle. They are sections of the two plots in Fig. 1 for different fixed values of the incident electron energy E_i . It is seen from Fig. 5 that the M1 cross section (continuous curves) is larger than the E2 cross section (dashed curves) in the whole kinematical region for small incident energies $E_i < 30$ MeV. Above this energy the E2 response is dominant for almost any angle, except for very small (forward) or very large (backward) angles. One can check that the crossing point of the two curves at small angles is characterized by $(qR)^2 \approx V_T$ for different incident energies.

Thus, the qualitative estimate (20) is not confirmed and the M1 response is dominant up to a much higher momentum transfer than predicted by PWBA.

Small scattering angles are not favourable for the study of nuclear excitations through inelastic electron scattering because of the large background originating from the radiative tail of the strong elastic peak [19, 7, 1]. On the other hand, a technique was developed for precise measurement of the inelastic cross section relative to the elastic peak, which can not be applied for backward angles [1]. There are many other sources of radiative background, contributing at 180° as well. Among them, the magnetic bremsstrahlung is particularly strong [1]. We turn our attention to the backward direction where most of the experiments on magnetic excitations have been done.

Let us check the estimates (17)-(20) in the case of backward scattering where the dominant longitudinal contribution is strongly damped by the kinematics. The expression (5) for the kinematic factor V_T diverges at 180° . Its correct limiting behaviour [21] can be obtained from Eqs. (4-12b,c) of [7] by taking the electron rest mass in the expression for V_ℓ into account. The transverse factor V_t (5) does not need such a correction at backward angles, so that,

$$V_\ell^e = \frac{\cos^2(\theta/2) + (m_e c^2)^2 / (E_i E_f)}{4 \sin^4(\theta/2)}, \quad 2V_T^e = \frac{1 + \sin^2(\theta/2)}{\cos^2(\theta/2) + (m_e c^2)^2 / (E_i E_f)}, \quad (22)$$

$$V_T^e(180^\circ) = \left(\frac{E_i}{m_e c^2} \right)^2 = 2V_T(0^\circ), \quad (23)$$

where $V_T(0^\circ)$ is given by (10). The upper index "e" is to remind that the electron mass was taken into account. The corrected factors (22) differ from the rough estimate (5) only for small incident energies and angles close to 180° . One obtains from (19), (20) and (23) for a full backward angle:

$$\begin{aligned} \frac{d\sigma(CL)}{d\sigma(EL, \text{conv})}(180^\circ) &\approx \left(\frac{2m_e c^2}{E_x} \right)^2, \\ \frac{d\sigma(CL)}{d\sigma(M, L-1)}(180^\circ) &\approx (2Mm_e c^4)^2 \left(\frac{R}{\hbar c} \right)^4 \approx 1.1. \end{aligned} \quad (24)$$

It is seen from (24) that the C2 and M1 cross sections should be of comparable magnitude even in fully backward scattering. The dominant contribution arises however from the transverse convection E2 response. According to (24), this contribution should be one order of magnitude larger than the longitudinal C2 cross section for the considered excitation energies $E_x \approx 3$ MeV.

The above qualitative PWBA estimates have been made without disposing of any information about the dynamics of the considered nuclear excitations. Let us compare them with our PWBA results obtained from the realistic RPA transition densities of the studied orbital 1^+ excitations in heavy deformed nuclei. The PWBA cross sections are plotted in Fig. 6 for $\theta = 179.5^\circ$. The M1 cross section arising from the convection current alone (dashed curve) is shown in the upper plot together with the total (convection plus spin, continuous curve) M1 cross section. It is seen that the M1 response is almost purely orbital for small momentum transfer, but the spin M1 contributions become larger for $q > 1.4 \text{ fm}^{-1}$.

The PWBA E2 cross sections, displayed in the lower plot of Fig. 6, demonstrate that the C2 response is already negligible at this large angle. The transverse E2 cross section is almost two orders of magnitude smaller than the M1 cross section for small momentum transfer q . These results, obtained from a realistic RPA wave function, stand in contrast with the general PWBA expectations (24) where the nuclear dynamics is not taken into account. According to (24), the transverse E2 excitation arising from the convection current should dominate over the M1 and C2 responses for small q in backward scattering.

The displayed cross sections are calculated with the simple kinematic factors (5) but the above conclusions are not altered when the more precise longitudinal factor V_ℓ^e (22) is used instead of V_ℓ to calculate the C2 cross section from the bottom plot of Fig. 6. The two expressions differ considerably only for small incident energies and angles very close to 180° . But even for $\theta = 179.5^\circ$ and realistic incident energies $E_i > 20 \text{ MeV}$ the largest discrepancy (for $E_i = 20 \text{ MeV}$) is not very relevant. The correct longitudinal factor V_ℓ^e (22) is about 40 times larger than the rough value (5), but V_ℓ^e is still 1270 times smaller than the transverse factor V_t . Thus, also with the correct factor V_ℓ^e the situation characterized by a negligible longitudinal response is not altered: the C2 contribution is still one order of magnitude smaller than the E2 cross section for small q ($E_i < 10 \text{ MeV}$).

4 PWBA analysis for large momentum transfer

The intensity of the scattered electrons decreases several orders of magnitude in the backward direction but this kinematical region is more interesting because the maximal momentum is transferred there for a given incident energy, as seen from (7). One can investigate in this way the high- q region, far from the photon point which could be studied also with more precise methods as photonuclear reactions [22].

The contribution of the Bessel functions to the form factors (4) are approximated in the high- q limit [7] by $j_L(qR) \sim 1$. This corresponds to $q > 0.15 \text{ fm}^{-1}$ for the considered rare-earth nuclei. Let us assume additionally that $q > 0.27 \text{ fm}^{-1}$, see Eq. (12), so that the leading convection and spin terms in the transverse EL and $ML-1$ form factors have the same q -dependence. The estimates (13) acquire now the simpler form:

$$\begin{aligned} |F_L^C(q)|^2 &\sim 1, \\ |F_L^E(q)|^2 &\sim |F_{L-1}^M(q)|^2 \sim \left(\frac{q\hbar c}{Mc^2}\right)^2. \end{aligned} \quad (25)$$

One obtains from (25) and (11) the following estimates for the PWBA cross sections for large momentum transfer:

$$d\sigma(CL) \sim q^{-2}W_\ell, \quad d\sigma(EL) \sim d\sigma(M, L-1) \sim \left(\frac{\hbar c}{Mc^2}\right)^2 W_\ell, \quad (26)$$

$$\frac{d\sigma(EL)}{d\sigma(M, L-1)} \approx 1, \quad (27)$$

$$\frac{d\sigma(CL)}{d\sigma(EL)} \approx \frac{d\sigma(CL)}{d\sigma(M, L-1)} \approx \left(\frac{Mc^2}{q\hbar c}\right)^2 \frac{1}{V_T}, \quad (28)$$

$$\frac{d\sigma(CL)}{d\sigma(EL)}(180^\circ) \approx \frac{d\sigma(CL)}{d\sigma(M, L-1)}(180^\circ) \approx \left(\frac{Mm_e c^4}{2E_i^2}\right)^2, \quad (29)$$

where (23) and (6) were used to get (29). If we choose an angle where $V_T = 1$, the ratio (28) is always a large number since $q < Mc^2/(\hbar c) = 4.75 \text{ fm}^{-1}$. This is indeed the condition for validity of the non-relativistic treatment of the nucleus [19]. One can conclude in this way from the estimates (27), (28), that the transverse $E2$ and $M1$ cross sections should be of comparable magnitude, while the longitudinal $C2$ excitation should dominate over them for not very large backward angles.

The prediction (28) is confirmed in Fig. 5 where the $E2$ response (mainly longitudinal $C2$) dominates over $M1$ for large q ($E_i > 30 \text{ MeV}$) apart from very large backward angles. This qualitative conclusion is confirmed also in Fig. 4, where the relative magnitudes of

the form factors are clearly seen due to $V_T = 1$. The longitudinal C2 dominates over the transverse E2 and M1 responses in Fig. 4 for large transferred momentum. Let us remind that the C2 dominance over the transverse E2 excitation, predicted by (19) for low q , was confirmed in the previous section, i.e. this relationship is valid for a wide region of transferred momenta.

The longitudinal dominance over the transverse currents is usually considered as a signature for collective excitations [5, 8]. One should note, however, that this dominance is predicted by Eqs. (19), (20) and (28), which are not restricted by any assumptions about the nature or extent of collectivity of the nuclear transition. On the other hand, collective excitations have been associated usually with the assumption for an irrotational, incompressible flow [9], whose signature is the vanishing transverse electric current $\hat{\mathcal{J}}_{L,L+1,M}(r)$ (34). Our RPA transition densities for the transverse E2 currents with $L' = L - 1$ and $L' = L + 1$ are of comparable magnitude (not in favour of collectivity according to the latter criterium) but their amplitude is one order of magnitude smaller than the amplitude of the C2 transition density (in favour of collectivity according to the former criterium). On the basis of different considerations we came to the conclusion [15, 12] that the low-lying orbital 1^+ excitations represent a weakly collective scissor mode.

In contrast to the validity of (28), the relationship (27), which should hold for any angle, is not confirmed by realistic results. Decomposition is made in Figs. 4 and 6 for 70.53° and 179.5° , respectively. It is seen from these two figures that for large q the transverse E2 excitation (mainly convection) is almost two orders of magnitude smaller than the M1 response (also mainly convection). It was found in the previous section that the corresponding prediction (18) for this ratio at low q contradicts our realistic results in the same way, but the discrepancy is three orders of magnitude for small momentum transfer.

The condition of M1 dominance over the C2 response for full backward scattering and for large q is obtained from (29): $E_i^2 > Mm_e c^4/2$ or $E_i > 15.5$ MeV. This estimate is confirmed in Fig. 6, where PWBA cross sections for $\theta = 179.5^\circ$ are displayed. They are obtained with realistic RPA transition densities. The lower plot shows that the transverse E2 contribution dominates over the C2 cross section. It is seen from the comparison of the two plots that also the M1 response dominates over the C2 excitation, as expected

from (29). The upper plot demonstrates that the M1 response is almost purely orbital for $q < 1.4 \text{ fm}^{-1}$: it originates mainly from the convection current (dashed curve). The spin M1 current becomes more important above this momentum transfer. This is due to the fact that the convection transition density is peaked close to the nuclear surface (at $r = 5 \text{ fm}$) and almost vanishes for $r < 2 \text{ fm}$, while the spin transition density has an appreciable amplitude also deep inside the nucleus, a region reached at high momentum transfer.

It has been argued [1, 2] that the spin-flip M1 response should dominate in backward scattering when the electron rest mass can be neglected in comparison with its incident energy and the transferred momentum is much larger than the nuclear excitation energy. These approximations are reasonable in backward scattering for not very small incident energy. In this case the electron can be viewed as a massless particle with a good helicity [23], i.e. it is longitudinally polarized and the electron spin is aligned along or opposite to its momentum. The scattering to 180° is considered in Ref. [1] as an occurrence of spin-flip, so that the longitudinal and transverse convection parts of the interaction should be strongly damped and only transverse spin M1 and spin E2 interactions will compete.

The ratio of the corresponding cross sections is given by the PWBA estimates (17) for small q and (27) for large q . Hence, if only transverse spin interactions had to compete with each other, a dominant spin M1 response could be expected from the above helicity arguments only for small $q < 0.15 \text{ fm}^{-1}$ where the necessary high-momentum approximation is not justified very well. Moreover, so small q -values are not reached in the (e, e') experiments [3, 4] investigating M1 excitations in heavy deformed nuclei, where $E_i \geq 20 \text{ MeV}$ or $q \geq 0.2 \text{ fm}^{-1}$ in backward scattering. The spin M1 and E2 cross sections should be almost equal at high q according to (27).

Inspection of Fig. 6 demonstrates that in backward scattering (negligible longitudinal response) the convection M1 cross section is much larger than the transverse E2 contribution even for large momentum transfer up to $q = 1.2 \text{ fm}^{-1}$. In this way, both the qualitative PWBA prediction (27) and the above helicity arguments for a dominant spin M1 response contradict the realistic results for the considered orbital M1 transition. The equality of the transverse M1 and E2 cross sections is predicted in (27) to take place for any $q > 0.15 \text{ fm}^{-1}$ while it is reached in reality for a much higher momentum transfer $q = 1.2 \text{ fm}^{-1}$. It is true that the longitudinal interaction is strongly suppressed in

backward scattering. This is easily seen from the small longitudinal kinematic factor V_ℓ^e (22). It is also true that high-energy electrons are longitudinally polarized. But even in the PWBA treatment of backward scattering of longitudinally polarized electrons both convection and spin currents contribute on equal footing to the cross section [24].

Let us compare finally the M1 and E2 DWBA cross sections plotted in Fig. 7 versus the effective momentum transfer q_{eff} (6) for different scattering angles. The M1 cross section is larger than the E2 contribution in the whole region of incident energies studied ($E_i < 210$ MeV) for small forward angles $\theta \leq 5^\circ$ (not shown in the figure, but seen in Fig. 1). At larger scattering angles there is always a crossing point for a given momentum transfer, beyond which the E2 response is dominant. The q -value of the crossing point obeys the relationship discussed in the previous section.

It is seen from Fig. 7 that the large q -values lie beyond the crossing point where the E2 excitation (mainly longitudinal) is dominant over M1. However, the crossing point moves towards higher q -values when approaching the backward direction, so that the M1 response becomes more important even for moderately large momentum transfer. The two cross sections decouple only at 175° . At this angle the M1 excitation dominates up to $q_{\text{eff}} = 1.3 \text{ fm}^{-1}$, while the C2 and the transverse E2 responses are of comparable magnitude. The C2 contributions are negligible beyond 175° and the total cross section is determined only by the relative transverse M1 and E2 responses which are multiplied by the same transverse factor V_t (5).

Cross sections of lower multipolarity decrease faster for larger q [5]. According to (14), the cross sections obey the following order of increasing multipolarity in their momentum dependence: $d\sigma(M, L-1) \sim (qR)^{2(L-2)}$, $d\sigma(CL) \sim (qR)^{2(L-1)}$, $d\sigma(EL) \sim (qR)^{2L}$, where the high- q limit, common for convection and spin transverse electric responses, is chosen. In addition to this general trend, our RPA results show that the studied orbital excitations have typical convection M1 transition densities similar to the charge C2 transition density: they are characterized by a well-localized single bump. In contrast, the spin M1 and transverse E2 transition densities exhibit more oscillations. Hence, the spin M1 response decreases less for larger q in comparison with the convection M1 term, i.e. the spin response behaves effectively as a higher multipolarity with respect to q .

One should expect, therefore, that the transverse E2 response will dominate over the

transverse M1 excitation for very large transferred momenta. This can be seen in the two bottom plots of Fig. 7 for $q_{\text{eff}} > 2 \text{ fm}^{-1}$. Thus, the transverse E2 response will be dominant even in a fully backward scattering for very large momentum transfer.

5 Summary

We have studied the (e, e') cross sections of low-lying excitations with $K^\pi = 1^+$ in heavy deformed nuclei. They have a predominantly orbital nature, in contrast to the more extensively explored spin-flip M1 excitations in spherical nuclei. Moreover, we have found recently [10, 11] that the accompanying E2 transitions with $I^\pi K = 2^+1$ provide appreciable contributions to the measured M1 cross sections in heavy deformed nuclei even in backward scattering where the M1 response is expected to dominate.

We obtain the cross sections from realistic microscopic RPA transition densities. The low-lying 1^+ excitation with the strongest orbital M1 transition in ^{156}Gd is studied as a typical example for such excitations which have been interpreted as a weakly collective scissors mode [15, 12]. The already reported good agreement [10, 11] of the theoretical DWBA cross sections with the available experimental data ($\theta = 165^\circ$) confirms the importance of the accompanying E2 transitions in heavy deformed nuclei and places some confidence in the validity of the theoretical cross sections for different scattering conditions.

The dependence of the theoretical M1 and E2 DWBA cross sections upon the scattering angle θ and the incident electron energy E_i is studied here in the whole kinematical region $0^\circ < \theta < 180^\circ$ for $10 \leq E_i \leq 210 \text{ MeV}$. In some special cases the cross sections are calculated also within PWBA in order to separate longitudinal from transverse contributions (not possible in DWBA). The DWBA and PWBA cross sections, obtained from realistic RPA transition densities, are compared to qualitative PWBA predictions which ignore completely the nuclear dynamics. They are based on general considerations of the scattering kinematics and the momentum dependence of the unknown form factors. The latter are fully specified by our RPA transition densities which is the main advantage of the microscopic approach.

The theoretical cross sections exhibit the following peculiarities in agreement with the

qualitative PWBA predictions:

i) For a given momentum transfer and $\theta > 90^\circ$ the (purely transverse) M1 cross section is almost constant with θ , while the E2 cross section decreases fast in the backward direction. This effect is simply due to the interplay between the longitudinal and transverse kinematic factors.

ii) For small momentum transfer q and a fixed scattering angle θ the transverse convection M1 and E2 cross sections are almost independent of q , while the longitudinal C2 cross section increases as q^2 . The convection current is dominant in the transverse E2 response for small q .

iii) The longitudinal C2 (Coulomb) form factor is much larger than the transverse M1 and E2 form factors. Therefore, the C2 response is dominant if the longitudinal kinematic factor is not very small. This condition is met away from the extreme forward and backward directions. Even for very small angles the Coulomb suppression is no more effective at high incident energies because of the momentum dependence in the kinematic factor.

iv) For scattering angles close to 180° , where the Coulomb response is negligible, the transverse E2 excitation dominates over the M1 transition at high transferred momenta. This is due to the fact that cross sections of lower multipolarity decrease faster with the increase in q .

The longitudinal dominance over the transverse currents is usually considered as a signature for collective excitations. However, this dominance is predicted in PWBA by Eqs. (19), (20) and (28), whose derivation does not involve any assumptions about the nature or extent of collectivity of the nuclear transition.

The PWBA predictions are not able to provide reliable numerical estimates for the limiting values of angles, incident energies and transferred momenta which specify the validity range of different predicted relationships. The qualitative PWBA estimates are either not able to predict or contradict the following realistic microscopic results for low-lying orbital 1^+ excitations:

v) The ratio between the C2 and M1 cross sections is three orders of magnitude smaller than estimated in PWBA. The PWBA predictions for a strong Coulomb response could be more appropriate for rotational transitions but not for the orbital M1 excitations

considered here. Thus, a more pronounced M1 dominance is present in our results at small momentum transfer, especially in backward scattering. The M1 response is dominant at any angle for incident energies $E_i < 30$ MeV. It is dominant in the forward direction, e.g. for $E_i < 150$ at $\theta = 1^\circ$ and even up to larger energies at smaller angles.

vi) The longitudinal C2 excitation is comparable with the transverse E2 response at $\theta = 175^\circ$ but becomes negligible beyond this angle in the backward direction. For such large angles the total cross section is determined by the interplay between transverse M1 and E2 excitations.

vii) In backward scattering ($175^\circ < \theta < 180^\circ$) the transverse M1 response is stronger than the transverse E2 excitation up to $q = 1.2 \text{ fm}^{-1}$. This feature stands in contrast to the qualitative PWBA predictions for a dominant transverse E2 transition in both low- and high- q regions (the latter refers to $q > 0.15 \text{ fm}^{-1}$). The two cross sections are comparably large in the region $1.2 < q < 2 \text{ fm}^{-1}$ and the transverse E2 cross section is expected to dominate for $q > 2 \text{ fm}^{-1}$ ($E_i > 200$ MeV in backward scattering).

viii) The M1 response originates mainly from the convection current up to $q = 1.4 \text{ fm}^{-1}$. The spin M1 current becomes more important above this momentum transfer due to the volume character of the oscillating spin M1 transition density.

The above properties apply to the low-lying 1^+ excitations in heavy deformed nuclei studied here. They are mainly orbital with small spin contributions. Such typical properties can not be predicted without information about the wave function of the considered nuclear excitation. Though high-energy electrons can be viewed as longitudinally polarized massless particles with a good helicity, there is no suppression of the convection current interaction in backward scattering. This is confirmed by the studied orbital excitations where the convection current provides the main contribution to the M1 response up to a high momentum transfer.

Thanks are due to Henk P. Blok and Jochen Heisenberg for providing us with their DWBA code and useful communications on the underlying formalism. This work is supported by the Deutsche Forschungsgemeinschaft (DFG) under contracts Fa 67/15-1 and Fa 67/15-2.

Appendix

The transition densities (2), (3) are calculated with the RPA wave functions in the laboratory frame in the way described in [17] for M1 transitions. In the case of E2 transitions they have the form:

$$\rho_2^\nu(r) = \frac{1}{2} \sum_{0 < i < f} \left[F_{+1}^\nu(fi) \rho_{21}(fi, r) + F_{+1}^\nu(f\tilde{i}) \rho_{21}(f\tilde{i}, r) \right], \quad (30)$$

$$\mathcal{J}_{2L'}^\nu(r) = \frac{1}{2} \sum_{0 < i < f} \left[F_{-1}^\nu(fi) \mathcal{J}_{2L'}(fi, r) + F_{-1}^\nu(f\tilde{i}) \mathcal{J}_{2L'}(f\tilde{i}, r) \right], \quad (31)$$

where the summation runs over single-particle states of the Woods-Saxon potential with projections K on the nuclear symmetry axis z obeying $0 < K_i < K_f$ and time-reversed states \tilde{i} are treated explicitly. The nuclear dynamics is contained in the factors F_σ^ν , $\sigma = \pm 1$, which are linear combinations of the RPA forward- and backward-going amplitudes $\psi_\nu(fi, m)$ and $\phi_\nu(fi, m)$ [15], respectively:

$$F_\sigma^\nu(fi) = \sqrt{2} \left[F_\sigma^\nu(fi, -1) - F_\sigma^\nu(fi, +1) \right], \quad (32)$$

$$F_\sigma^\nu(fi, m) = \psi_\nu(fi, m) + \sigma m \phi_\nu(fi, m), \quad (33)$$

The signature index $m = \pm 1$, corresponding to the indistinguishable x and y directions, is of technical interest only. It allows us to take symmetries into account and to avoid the problem of symmetrizing the momentum operator [19]. Final results do not depend on the signature, as seen from (30), (31). In order to save space we skip in (32), (33) and below expressions involving time-reversed initial states \tilde{i} , though we always take such terms in the numerical calculations into account.

The notations $\rho_{21}(fi, r)$ in (30) and $\mathcal{J}_{2L'}(fi, r)$ in (31) stand for the q.p. matrix elements of the E2 charge and current density operators $\hat{\rho}_{21}(r)$ and $\hat{\mathcal{J}}_{2L'}(r)$, respectively:

$$\hat{\rho}_{21}(r) = \int Y_{21}(\Omega) \hat{\rho}(\mathbf{r}) d\Omega, \quad \hat{\mathcal{J}}_{2L'}(r) = \int \mathbf{Y}_{2L'}(\Omega) \bullet \hat{\mathbf{J}}(\mathbf{r}) d\Omega, \quad L' = 1, 3, \quad (34)$$

$\mathbf{Y}_{LL'M}(\Omega)$ are the vector spherical harmonics [25]. The nuclear charge and current density operators $\hat{\rho}(\mathbf{r})$ and $\hat{\mathbf{J}}(\mathbf{r})$ can be found, e.g. in [7, 17, 19].

The q.p. matrix elements are obtained with the help of the eigenfunctions Φ_i of the deformed Woods-Saxon potential [26] in cylindrical coordinates (ρ, z, φ) :

$$\Phi_i(K^\pi, \mathbf{r}) = \sum_j C_j^i \Psi_j(n_\rho, n_z, \Lambda, \Sigma = \frac{1}{2}, K, \mathbf{r})$$

$$\begin{aligned}
& + \sum_{j'} C_{j'}^i \Psi_{j'}(n'_\rho, n'_z, \Lambda' = \Lambda + 1, \Sigma' = -\frac{1}{2}, K, \mathbf{r}), \\
\Psi(n_\rho, n_z, \Lambda, \Sigma, \mathbf{r}) &= \psi^\Lambda(n_\rho, \rho) \psi(n_z, z) \psi(\Lambda, \varphi) \chi(\Sigma),
\end{aligned} \tag{35}$$

where C_j^i , $j = (n_\rho, n_z)$, are the coefficients of the expansion over the basis wave functions Ψ_j of the axially symmetric harmonic oscillator. The cylindrical quantum numbers n_z , n_ρ , correspond to the directions along and perpendicular to the symmetry axis, while $\Lambda = K - 1/2$ and Σ are the projections of the orbital angular momentum and spin operators on this axis. The angular integration over $d\Omega = \sin\theta d\theta d\varphi$ in (30), (31), reduces to integration over $-d\cos\theta$ since the integration over the azimuth angle φ and the spin matrix elements can be performed analytically in the basis (35). One obtains in this way the following expressions for the q.p. matrix elements of the charge transition density (30):

$$\begin{aligned}
\rho_{21}(fi, r) &= eU_{+1}(f, i) \int Y_{21}(\Omega) \Phi_f^\dagger(\mathbf{r}) \Phi_i(\mathbf{r}) d\Omega \\
&= -eU_{+1}(f, i) \sqrt{\frac{15}{8\pi}} \sum_{\Lambda'=\Lambda, \Lambda+1} \int \frac{\rho z}{r^2} A^{fi}(\Lambda' + 1, \Lambda') d\cos\theta, \\
&\quad \rho = r \sin\theta, \quad z = r \cos\theta,
\end{aligned} \tag{36}$$

where the coefficients U_{+1} are linear combinations of the BCS occupation numbers. The functions A^{fi} contain only $\psi^\Lambda(n_\rho, \rho) \psi(n_z, z)$ from (35). Thus, they depend only on z and ρ , i.e. they are products of Hermite and associate Laguerre polynomials [27]:

$$\begin{aligned}
U_\sigma(f, i) &= u_f v_i + \sigma u_i v_f, \quad \sigma = \pm 1, \\
A^{fi}(\Lambda_f, \Lambda_i) &= \sum_{kj} C_k^f(\Lambda_f) C_j^i(\Lambda_i) \psi_k^{\Lambda_f}(\rho) \psi_j^{\Lambda_i}(\rho) \psi_k(z) \psi_j(z).
\end{aligned} \tag{37}$$

The q.p. matrix elements of the transverse E2 convection currents have the form:

$$\begin{aligned}
\mathcal{J}_{211}^C(fi, r) &= i\mu_N U_{-1}(f, i) \frac{1}{2} \sqrt{\frac{3}{\pi}} \sum_{\Lambda'=\Lambda, \Lambda+1} \int \left\{ \frac{z}{r} \left[\frac{\partial}{\partial \rho_i} A^{fi}(\Lambda' + 1, \Lambda') \right. \right. \\
&\quad \left. \left. - \frac{\Lambda'}{\rho} A^{fi}(\Lambda' + 1, \Lambda') \right] + \frac{\rho}{r} \frac{\partial}{\partial z_i} A^{fi}(\Lambda' + 1, \Lambda') \right\} d\cos\theta,
\end{aligned} \tag{38}$$

$$\begin{aligned}
\mathcal{J}_{231}^C(fi, r) &= \frac{i\mu_N}{\sqrt{2\pi}} U_{-1}(f, i) \sum_{\Lambda'=\Lambda, \Lambda+1} \int \left\{ \frac{(z^2 - 4\rho^2)}{r^3} \left[z \frac{\partial}{\partial \rho_i} + \rho \frac{\partial}{\partial z_i} \right] A^{fi}(\Lambda' + 1, \Lambda') \right. \\
&\quad \left. - \frac{z\Lambda'}{r\rho} A^{fi}(\Lambda' + 1, \Lambda') \right\} d\cos\theta,
\end{aligned} \tag{39}$$

where the factors $U_{-1}(f, i)$ are defined in (37). The notations $\partial \rho_i$ and ∂z_i mean that only the wave functions of the initial state in A^{fi} must be differentiated.

The transverse E2 magnetization currents give rise to the following q.p. matrix elements:

$$\begin{aligned} \mathcal{J}_{211}^S(fi, r) = ig^s \mu_N U_{-1}(f, i) \frac{1}{8} \sqrt{\frac{3}{\pi}} \int \left\{ \frac{z}{r} \left[\left(\frac{\partial}{\partial \rho} - \frac{1}{\rho} \right) [A^{fi}(\Lambda + 1, \Lambda) - A^{fi}(\Lambda + 2, \Lambda + 1)] \right. \right. \\ \left. \left. + 2 \frac{\partial}{\partial z} A^{fi}(\Lambda + 1, \Lambda + 1) \right] \right. \\ \left. + \frac{\rho}{r} \left[\frac{\partial}{\partial \rho} [A^{fi}(\Lambda + 1, \Lambda + 1) - A^{fi}(\Lambda + 2, \Lambda)] + \frac{2}{\rho} A^{fi}(\Lambda + 2, \Lambda) \right] \right\} d \cos \theta, \quad (40) \end{aligned}$$

$$\begin{aligned} \mathcal{J}_{231}^S(fi, r) = \frac{ig^s \mu_N}{4\sqrt{2\pi}} U_{-1}(f, i) \int \left\{ \frac{z}{r} \frac{\partial}{\partial \rho} [A^{fi}(\Lambda + 1, \Lambda) - A^{fi}(\Lambda + 2, \Lambda + 1)] \right. \\ \left. + \frac{(z^2 - 4\rho^2)}{r^3} \left[\rho \frac{\partial}{\partial \rho} [A^{fi}(\Lambda + 2, \Lambda) - A^{fi}(\Lambda + 1, \Lambda + 1)] \right. \right. \\ \left. \left. - 2A^{fi}(\Lambda + 2, \Lambda) + \frac{z}{\rho} [A^{fi}(\Lambda + 1, \Lambda) - A^{fi}(\Lambda + 2, \Lambda + 1)] \right] \right. \\ \left. - \frac{z}{r^3} \left[(2z^2 - 3\rho^2) \frac{\partial}{\partial z} A^{fi}(\Lambda + 1, \Lambda + 1) + 5\rho^2 \frac{\partial}{\partial z} A^{fi}(\Lambda + 2, \Lambda) \right] \right\} d \cos \theta, \quad (41) \end{aligned}$$

where g^s are the spin gyromagnetic ratios (1). All differentiations in (38)-(41) are performed analytically [17] using recurrency relations for Hermite and Laguerre polynomials. The numerical integration in (36) and (38)-(41) extends over $0 \leq \cos \theta \leq 1$.

References

- [1] L. W. Fagg, Rev. Mod. Phys. 47 (1975) 683
- [2] S. Raman, L. W. Fagg and R. S. Hicks, Internat. Rev. Nucl. Phys. 7 (1991) 355
- [3] D. Bohle, A. Richter, W. Steffen, A. E. L. Dieperink, N. Lo Iudice, F. Palumbo and O. Scholten, Phys. Lett. B137 (1984) 27
- [4] A. Richter, Nucl. Phys. A522 (1991) 139c; A553 (1993) 417c; Progr. Part. Nucl. Phys. 34 (1995) 261
- [5] W. C. Barber, Ann. Rev. Nucl. Sci. 12 (1962) 1
- [6] W. C. Barber, J. Goldemberg, G. A. Peterson and Y. Torizuka, Nucl. Phys. 41 (1963) 461
- [7] H. Überall, Electron Scattering from Complex Nuclei (Academic Press, New York, London, 1971)
- [8] J. Heisenberg and H. P. Blok, Ann. Rev. Nucl. Part. Sci. 33 (1983) 569
- [9] J. Heisenberg, Adv. Nucl. Phys. 12 (1981) 61
- [10] R. Nojarov, A. Faessler and M. Dingfelder, J. of Phys. G20 (1994) L111
- [11] M. Dingfelder, R. Nojarov and A. Faessler, Progr. Part. Nucl. Phys. 34 (1995) 319
- [12] R. Nojarov, Progr. Part. Nucl. Phys. 34 (1995) 297
- [13] D. Bohle, A. Richter, K. Heyde, P. Van Isacker, J. Moreau and A. Sevrin, Phys. Rev. Lett. 55 (1985) 1661
- [14] R. Nojarov, A. Faessler and M. Dingfelder, Phys. Rev. C51 (1995) 2449
- [15] R. Nojarov and A. Faessler, Nucl. Phys. A484 (1988) 1
- [16] D. Bohle, A. Richter, U. E. P. Berg, J. Drexler, R. D. Heil, U. Kneissl, H. Metzger, R. Stock, B. Fischer, H. Hollick and D. Kollewe, Nucl. Phys. A458 (1986) 205
- [17] A. Faessler, R. Nojarov and T. Taigel, Nucl. Phys. A492 (1989) 105

- [18] M. Petraitis, J. P. Connelly, Hall Crannell, L. W. Fagg, J. T. O'Brien, D. I. Sober, J. R. Deininger, S. E. Williamson, R. Lindgren and S. Raman, Phys. Rev. C49 (1994) 3000
- [19] R. S. Willey, Nucl. Phys. 40 (1963) 529
- [20] R. Raphael and H. Überall, Phys. Rev. 143 (1966) 671
- [21] H. Theissen, Springer Tracts in Mod. Phys. 65 (1972) 1
- [22] U. Kneissl, J. Margraf, H. H. Pitz, P. von Brentano, R.-D. Herzberg and A. Zilges, Progr. Part. Nucl. Phys. 34 (1995) 285
- [23] A. I. Ahieser, A. G. Sitenko and V. K. Tartakovskii, Elektrodinamika yader (Naukova Dumka, Kiev, 1989) p. 177
- [24] L. J. Weigert and M. E. Rose, Nucl. Phys. 51 (1964) 529
- [25] D. A. Varshalovich, A. N. Moskalev and V. K. Khersonskii, Quantum Theory of Angular Momentum (World Scientific, Singapore, 1988)
- [26] J. Damgaard, H.-C. Pauli, V. V. Pashkevich and V. M. Strutinski, Nucl. Phys. A135 (1969) 432
- [27] R. Nojarov, Z. Bochnacki and A. Faessler, Z. Phys. A324 (1986) 289

Figure 1: Upper plot: DWBA cross section of the strongest M1 excitation with $I^\pi K = 1^+1$ and $E_x^{\text{th}} = 2.9$ MeV in ^{156}Gd plotted versus the incident electron energy E_i and the scattering angle θ . Lower plot: DWBA cross section of the accompanying E2 excitation with $I^\pi K = 2^+1$. The (e, e') cross sections are obtained from the RPA transition densities (30), (31). The thick contour lines indicate orders of magnitude, while the dashed contour lines are drawn at 5 times the next lower order of magnitude.

Figure 2: The same as in Fig. 1 but the DWBA M1 and E2 cross sections are plotted versus the effective momentum transfer q_{eff} (6) instead of E_i .

Figure 3: PWBA E2 cross section of the same excitation as in Fig. 1 plotted versus the incident electron energy E_i for small scattering angles $\theta = 0.1^\circ, 0.5^\circ, 1^\circ$ and 5° . The total cross section (continuous curve) is a sum of the longitudinal C2 (dashed curve) and transverse E2 (dotted curve) contributions.

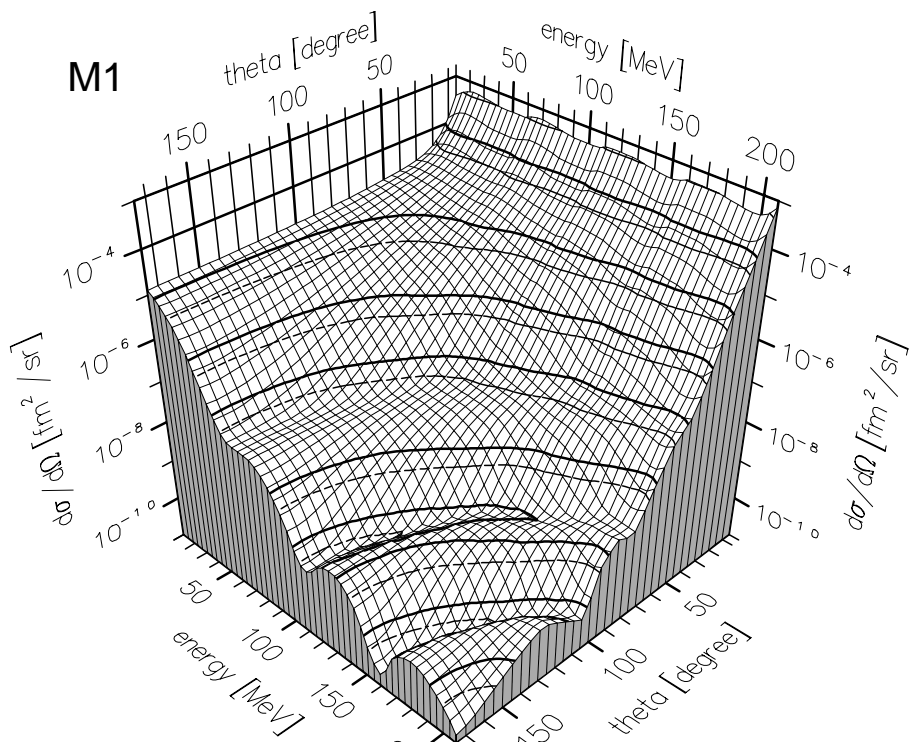
Figure 4: Cross sections for $\theta = 70.53^\circ$, where $V_T = 1$ from Eq. (5), so that each PWBA cross section is proportional to its form factor with the same coefficient. Upper two plots: PWBA cross sections versus momentum transfer q (6). Top plot: convection M1 (dashed curve) and total M1 (convection plus spin, continuous curve). Middle plot: longitudinal C2 (continuous curve) and transverse E2 (dashed curve). Bottom plot: DWBA cross sections versus q_{eff} (6); orbital M1 (long-dashed curve), total M1 (convection plus spin, continuous curve), and total E2 (longitudinal plus transverse, short dashed curve).

Figure 5: Comparison between M1 (continuous curves) and E2 (dashed curves) DWBA cross sections plotted versus the scattering angle θ . These are sections from the plots in Fig. 1 corresponding to different incident energies E_i , listed in each plot.

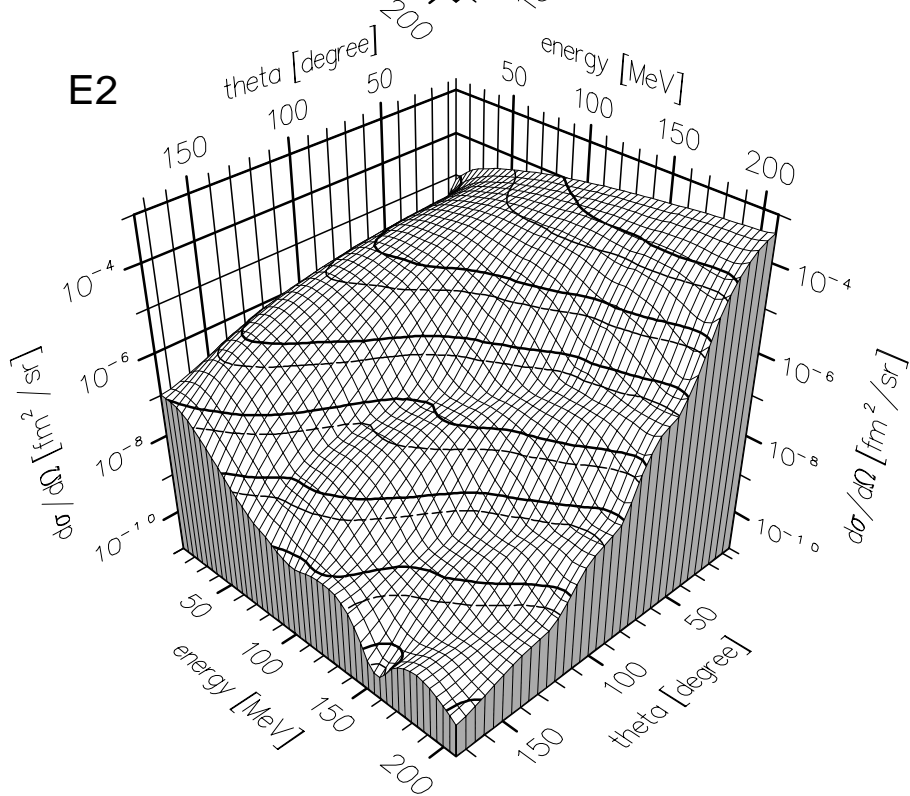
Figure 6: M1 (upper plot) and E2 (lower plot) PWBA cross sections for $\theta = 179.5^\circ$ versus momentum transfer q . Decomposition and notations as in the upper two plots of Fig. 4, respectively.

Figure 7: Comparison between M1 (continuous curves) and E2 (dashed curves) DWBA cross sections plotted versus the effective momentum transfer q_{eff} (6). These are sections from Fig. 2 for different scattering angles θ , listed in each plot.

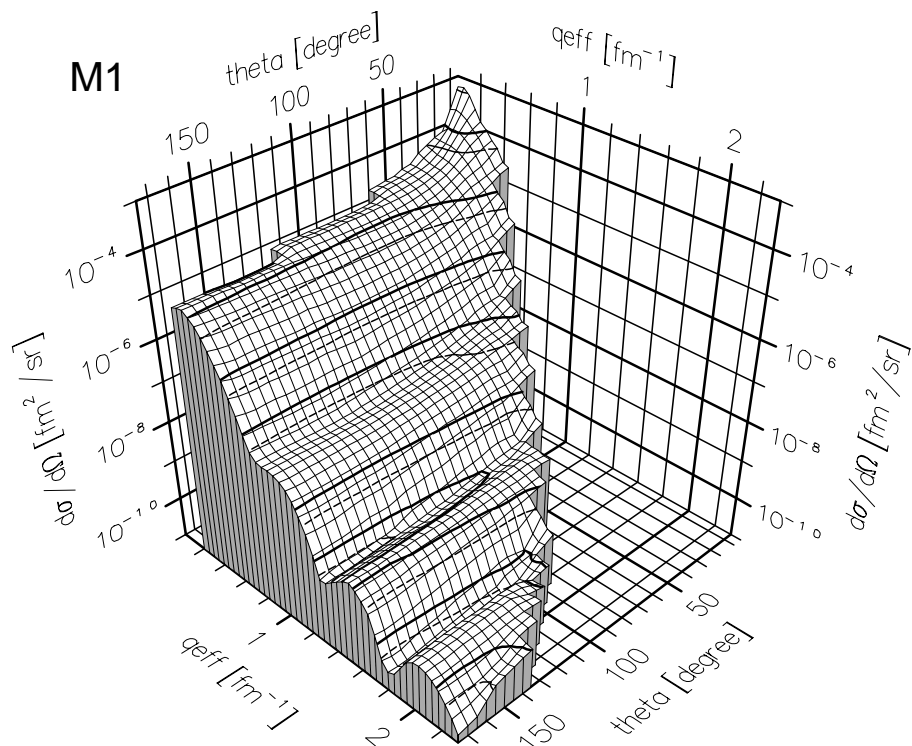
M1



E2



M1



E2

